

Reaction-Diffusion-Integral System Modeling SARS-CoV-2 Infection-Induced versus Vaccine-Induced Immunity: Analytical Solutions and Stability Analysis

Jeerawan Suksamran, Somkid Amornsamankul, Yongwimon Lenbury

Abstract— Understanding protection from SARS-CoV-2 infection and severe COVID-19 induced by natural SARS-CoV-2 infection versus vaccination is essential for informed vaccine mandate decisions. In this article, we construct a system of reaction-diffusion-integral equations to describe the development of vaccinated population, not previously infected, and pre-infected population, vaccinated or not, subject to continued exposure to coronavirus leading to possible re-infection. The model accounts for the differences in induced immunity in the two populations and the spread of infection due to movements of various populations in space. To realistically describe the nature of immunity, which has been found to decline with time following vaccination or infection, the rate of infection is expressed here as an integral of a function of the specific rate of infection that increases exponentially with time, depending on how long it is after the subjects have been infected with, or vaccinate against, the virus. The model is analyzed for its stability, and the contour plot is presented. The analytical solutions of the model system are derived in the form of traveling waves, using the modified extended hyperbolic tangent method. Inspection and interpretation of the different shapes of these plots yield valuable insights.

Index Terms—SAR-CoV-2 infection, infection-induced vs vaccination-induced immunity, reaction-diffusion-integral equations, travelling wave solutions.

Manuscript received June 26, 2023; revised November 13, 2023

This research has received funding support from the NSRF via the Program Management Unit for Human Resource & Institutional Development, Research and Innovation (grant number B05F640231), and partially supported by the Centre of Excellence in Mathematics, Ministry of Higher Education, Science, Research and Innovation, Thailand (grant number RG-01-65-01-1).

J. Suksamran is a lecturer at the Department of Mathematics, Faculty of Applied Science, King Mongkut's University of Technology North Bangkok, Bangkok 10800, Thailand. (phone: 094-946-1546; e-mail: jeerawan.tangmo@gmail.com).

S. Amornsamankul is a lecturer at the Department of Mathematics, Faculty of Science, Mahidol University, Rama 6 Rd., Bangkok 10400, Thailand, and the Centre of Excellence in Mathematics, MHESI, Bangkok, Thailand. (e-mail: somkid.amo@mahidol.ac.th).

Y. Lenbury is a lecturer at the Department of Mathematics, Faculty of Science, Mahidol University, Rama 6 Rd., Bangkok 10400, Thailand, and the Centre of Excellence in Mathematics, MHESI, Bangkok, Thailand. (e-mail: yongwimon.len@mahidol.ac.th).

I. INTRODUCTION

EVER since the outbreak of SAR-CoV-2, we have seen an exponential growth in research and publications devoted to its detection, for example in [1], the use of models and other advanced techniques to analyze its spread and prevalence, such as those reported in [2], [3] and [4], as well as utilizing Bayesian Logistic Regression and Naive Bayes Classifier [5] to classify death risk for COVID-19 patients.

Nations all across the globe have developed and mandated numerous public health measures to bring down the rate of transmission and control the pandemic [6]. Apart from the effort of the scientific research community to find better treatment strategies for the disease, intense research has been directed toward developing a safe and effective vaccine to reign in the spread of the disease [6].

According to Chemaitelly et al. [7], whether a person has been previously infected or not, vaccination still provides the safest and the best protection against infection and COVID-19-related hospitalization and death. In their recent report, Chemaitelly and his co-workers [7] went on to say that previous natural infection was correlated with lower incidence of coronavirus infection, whatever the variant, than mRNA primary-series vaccination. Although COVID-19 vaccines induce immunity against coronavirus infection and COVID-19-related hospitalization and morbidity, natural infection with the virus also induces immunity against renewed infection as well as COVID-19-related hospitalization and morbidity. An increasing number of investigations suggest that differences are evident in the level and persistence of protection provided by natural infection in comparison to vaccination [7] – [10]. Even more perplexing is the discovery that moderate to severe coronavirus infection induces immunity from vaccination more effectively than infection that is mild or asymptomatic [11].

In addition, it was concluded in [12] that immunity provided by vaccination or prior infection against SARS-CoV-2 infection wanes with time. Specifically, the immunity induced by vaccination against symptomatic coronavirus infection reduces to a quarter to a third of the original level within 6 months. On the other hand, the protection against symptomatic reinfection induced by pre-infection wanes at a slower rate, only slight declines being

observed one year later. Moreover, protection provided by both vaccination and prior infection against symptomatic infection was found to wane more rapidly than protection against severe, critical, or fatal infection [12].

However, there is still conflicting evidence in this regard, as voiced by Hernandez-Suarez in [13] that there are indications that protection provided by prior infection lasts longer only when compared to those patients who did not fulfill the complete dose.

Because of these conflicting reports, it becomes important for policy making purposes to be able to characterize how waning immunity affects the spread of SARS-CoV-2 infection over time and space, especially in choosing optimal vaccination strategies, testing policy, and readiness of health care facilities at the right time and location.

Due to insufficient empirical data and lack of conclusive evidence, mathematical modelling can play a crucial role in driving and testing policies. Models that reflect observed infection characteristics, such as the difference in immunity provided by prior infection versus vaccination, are needed to complement the knowledge that cannot be gleaned from data accumulation and analysis alone.

We therefore propose a model system of reaction-diffusion-integral equations to track the densities of infective individuals and those who are susceptible to infection, each divided into 2 groups, namely, those who have been vaccinated and those who have been previously infected. To model the decline in immunity, the rate of infection is written as an integral involving the specific infection rate that increases exponentially with time. The model will be analyzed for its stability, and the contour plot will be presented. The analytical solutions of the model system are then derived in the form of traveling waves, using the modified extended hyperbolic tangent method. The results of our analysis and simulations are interpreted to shed light onto how pre-infection and vaccination impact in varying degrees on subsequent infections and how waning immunity plays a role in the spread of SARS-CoV-2 infection over time and space.

II. MODEL SYSTEM

In order to discover the different manners in which SARS-CoV-2 infection spread through time and space within the population of susceptible individuals who have been vaccinated and that of individuals who have been previously infected, we divide the susceptible population into two groups, one of which consists of those individuals who have been vaccinated but have never been infected, and the other consists of those who have been previously infected, vaccinated or not, expected to have some infection-induced immunity. The infectious population is similarly divided into two groups. One of them consists of those individuals who get infected after they have been vaccinated, but have not been infected previously. The other group consists of those individuals who get infected after having been infected beforehand. Namely, we let

$I_v(x, t)$ = density of population of infected individuals derived from those having been vaccinated, but not previously infected,

$I_i(x, t)$ = density of population of infected individuals derived from those who have been infected previously, whether having been vaccinated or not,

$S_v(x, t)$ = density of susceptibles vaccinated at least once, not having been infected,

$S_i(x, t)$ = density of susceptibles having been infected, vaccinated or not,

$I_0(x, t)$ = density of population of infected individuals who are not members of either I_v or I_i population,

$S_0(x, t)$ = density of susceptibles having never been vaccinated or infected,

$$I(x, t) = I_0(x, t) + I_i(x, t) + I_v(x, t),$$

where t denotes the time, and x denotes the spatial radial distance measured from a point of reference at the center of the infected area. We then arrive at the following model equations.

$$\frac{\partial I_v}{\partial t} = \varepsilon_v \frac{\partial^2 I_v}{\partial x^2} + \alpha_v I \int_0^t (1 - e^{-\gamma_i(t-\tau)}) S_v(x, \tau) d\tau - d_v I_v - r_v I_v, \quad (1)$$

$$\frac{\partial I_i}{\partial t} = \varepsilon_i \frac{\partial^2 I_i}{\partial x^2} + \alpha_i I \int_0^t (1 - e^{-\gamma_i(t-\tau)}) S_i(x, \tau) d\tau - d_i I_i - r_i I_i, \quad (2)$$

$$\frac{\partial S_v}{\partial t} = \mu_v \frac{\partial^2 S_v}{\partial x^2} - \alpha_v I \int_0^t (1 - e^{-\gamma_i(t-\tau)}) S_v(x, \tau) d\tau + \nu S_0, \quad (3)$$

$$\frac{\partial S_i}{\partial t} = \mu_i \frac{\partial^2 S_i}{\partial x^2} - \alpha_i I \int_0^t (1 - e^{-\gamma_i(t-\tau)}) S_i(x, \tau) d\tau + r_0 I_0 + r_v I_v + r_i I_i, \quad (4)$$

$$\frac{\partial I_0}{\partial t} = \mu_i \frac{\partial^2 I_0}{\partial x^2} - d_0 I_0 - r_0 I_0, \quad (5)$$

$$\frac{\partial S_0}{\partial t} = \mu_s \frac{\partial^2 S_0}{\partial x^2} - \nu S_0. \quad (6)$$

The first term on the right of (1) is the rate of change of infected population density I_v due to spatial movement or migration of infected individuals, with diffusion constant ε_v representing the strength of contribution from such migration. The second term corresponds to the rate of increase in the infected population I_v due to the contact between the infectious individuals I and the susceptible individuals S_v , in which the integral term

$$G_1(x, t) \triangleq \int_0^t (1 - e^{-\gamma_i(t-\tau)}) S_v(x, \tau) d\tau \quad (7)$$

accounts for the decline in immunity of $S_v(x, t)$ the longer after they have been infected. When t is further from τ , $t - \tau$ is larger and the specific rate of infection, per unit of density of the infectious individuals per unit of density of susceptible individuals, $1 - e^{-\gamma_i(t-\tau)}$, is larger, which means the susceptible individuals $S_v(x, t)$ get infected more. On the other hand, when the elapsed time is small, $1 - e^{-\gamma_i(t-\tau)}$ becomes smaller, which means the susceptible individuals $S_v(x, t)$ get infected less. Thus, (7) accounts for the waning in vaccine-induced immunity observed in clinical data.

Similarly, the expression

$$G_2(x,t) \triangleq \int_0^t (1 - e^{-\gamma_i(t-\tau)}) S_i(x,\tau) d\tau \quad (8)$$

accounts for the decline in infection-induced immunity of $S_i(x,t)$. Such rate integrals representing exponential decline of this form have been described and utilized in earlier models in which the transmission strength declines with time [14], [15]. The coefficients α_v and α_i of these integral represent the strengths of the contributions from such infection from $S_v(x,t)$ and $S_i(x,t)$, respectively, while γ_v and γ_i are the corresponding decay constants. The last 2 terms in (1) are the removal rates due to death and recovery with specific rates d_v and r_v , respectively.

The terms on the right of (2), including the definitions of ε_i, d_i and r_i , follow in the similar manner as those in (1).

The first term on the right of (3) is the rate of change of susceptible population density S_v due to spatial movement or migration of susceptible individuals, with diffusion constant μ_v representing the strength of contribution from such migration. The second term corresponds to the rate of removal in S_v due to infection, and the last term is its increase due to infection of the population S_0 , taken to vary directly as its current density with constant of variation ν . The first 2 terms on the right of (4) and the coefficient μ_i follow in the similar manner as those in (3), while the last 3 terms are the rate of increase of S_i due to recovery from infection of I_0, I_v , and I_i , with specific rates r_0, r_v , and r_i respectively.

In (5) and (6), I_0 and S_0 increase due to migration, with strength coefficients μ_i and μ_s , respectively, and decrease due to death ($d_0 I_0$), recovery ($r_0 I_0$) or new infection (νS_0), where d_0, r_0 and ν are the respective specific rates of change. With equation (5), we assume that strict isolation is enforced once an individual, who has not been vaccinated or pre-infected, is infected, so that no movement is observed, so that we may put $\mu_i = 0$. It is then straightforward to show that $I_0 \rightarrow 0$, as $t \rightarrow \infty$. For S_0 in (6), those who have not been vaccinated or infected are expected to observe strict isolation, not moving around, since they cannot be assured of any immunity. We may then put $\mu_s = 0$, in which case we also have $S_0 \rightarrow 0$, as $t \rightarrow \infty$. We shall then consider the development in the levels of I_v, I_i, S_v , and S_i , in the situation where I_0 and S_0 have been depleted, and carry out our analysis on the model which consists of the following equations.

$$\frac{\partial I_v}{\partial t} = \varepsilon_v \frac{\partial^2 I_v}{\partial x^2} + \alpha_v I G_v - d_v I_v - r_v I_v, \quad (11)$$

$$\frac{\partial I_i}{\partial t} = \varepsilon_i \frac{\partial^2 I_i}{\partial x^2} + \alpha_i I G_i - d_i I_i - r_i I_i, \quad (12)$$

$$\frac{\partial S_v}{\partial t} = \mu_v \frac{\partial^2 S_v}{\partial x^2} - \alpha_v I G_v, \quad (13)$$

$$\frac{\partial S_i}{\partial t} = \mu_i \frac{\partial^2 S_i}{\partial x^2} - \alpha_i I G_i + r_v I_v + r_i I_i, \quad (14)$$

$$\frac{\partial^2 G_v}{\partial t^2} = -\gamma_v \frac{\partial G_v}{\partial t} + \gamma_v S_v, \quad (15)$$

$$\frac{\partial^2 G_i}{\partial t^2} = -\gamma_i \frac{\partial G_i}{\partial t} + \gamma_i S_i, \quad (16)$$

where equations (15) and (16) have been derived from differentiating G_v and G_i , respectively, with respect to time, assuming no contribution from migration.

In the next section, we shall carry out a stability analysis on the model system (11) – (16) to determine whether there exist some conditions under which the solution to our model remains close to, or tends asymptotically, to some steady state value.

III. STABILITY ANALYSIS

To determine dynamic or asymptotic behavior of the solutions to (11) – (16), we introduce the travelling wave coordinate, $\xi = x - ct$, which transforms (11) – (16) into the following system of ordinary differential equations.

$$-c i_v' = \varepsilon_v i_v'' + \alpha_v (i_v + i_i) g_v - d_v i_v - r_v i_v, \quad (17)$$

$$-c i_i' = \varepsilon_i i_i'' + \alpha_i (i_v + i_i) g_i - d_i i_i - r_i i_i, \quad (18)$$

$$-c s_v' = \mu_v s_v'' - \alpha_v (i_v + i_i) g_v, \quad (19)$$

$$-c s_i' = \mu_i s_i'' - \alpha_i (i_v + i_i) g_i + r_v i_v + r_i i_i, \quad (20)$$

$$c^2 g_v'' = \gamma_v c g_v' + \gamma_v s_v, \quad (21)$$

$$c^2 g_i'' = \gamma_i c g_i' + \gamma_i s_i, \quad (22)$$

where ()' stands for the derivative of the specific state variable with respect to ξ , and

$$i_v(\xi) = I_v(x,t), \quad i_i(\xi) = I_i(x,t), \quad s_v(\xi) = S_v(x,t),$$

$$s_i(\xi) = S_i(x,t), \quad g_v(\xi) = G_v(x,t), \quad g_i(\xi) = G_i(x,t).$$

The above system of second order differential equations can be transformed into a system of first order equations by letting

$$y_1 = i_v, x_1 = i_v', y_2 = i_i, x_2 = i_i', y_3 = s_v, x_3 = s_v',$$

$$y_4 = s_i, x_4 = s_i', y_5 = g_v, x_5 = g_v', y_6 = g_i, x_6 = g_i',$$

which yields

$$y_1' = x_1, \quad (23)$$

$$y_2' = x_2, \quad (24)$$

$$y_3' = x_3, \quad (25)$$

$$y_4' = x_4, \quad (26)$$

$$y_5' = x_5, \quad (27)$$

$$y_6' = x_6, \quad (28)$$

$$x_1' = \frac{d_v}{\varepsilon_v} y_1 + \frac{r_v}{\varepsilon_v} y_1 - \frac{\alpha_v}{\varepsilon_v} (y_1 + y_2) y_5 - \frac{c}{\varepsilon_v} x_1, \quad (29)$$

$$x_2' = \frac{d_i}{\varepsilon_i} y_2 + \frac{r_i}{\varepsilon_i} y_2 - \frac{\alpha_i}{\varepsilon_i} (y_1 + y_2) y_6 - \frac{c}{\varepsilon_i} x_2, \quad (30)$$

$$x_3' = \frac{\alpha_v}{\mu_v} (y_1 + y_2) y_5 - \frac{c}{\mu_v} x_3, \tag{31}$$

$$x_4' = \frac{\alpha_i}{\mu_i} (y_1 + y_2) y_6 - \frac{r_v}{\mu_i} y_1 - \frac{r_i}{\mu_i} y_2 - \frac{c}{\mu_i} x_4, \tag{32}$$

$$x_5' = \frac{\gamma_v}{c^2} y_3 + \frac{\gamma_v}{c} x_5, \tag{33}$$

$$x_6' = \frac{\gamma_i}{c^2} y_4 + \frac{\gamma_i}{c} x_6. \tag{34}$$

Equating the right hand sides of (23) – (34) to zero, we find steady states $\omega 1 = (0, \dots, 0, \tilde{y}_1, \tilde{y}_2, 0, \dots, 0)$, distributed on the (y_1, y_2) -plane, and $\omega 2 = (0, \dots, 0, 0, 0, \tilde{y}_5, \tilde{y}_6)$, distributed on the (y_5, y_6) - plane, where $\tilde{y}_1, \tilde{y}_2, \tilde{y}_5$, and \tilde{y}_6 can be any arbitrary positive values.

To discover the stability behavior of the system near a steady state $\omega 1$, for some fixed values c_1 of \tilde{y}_1 and c_2 of \tilde{y}_2 , we find the Jacobian matrix of the model system about $\omega 1$ to obtain the eigenvalues $\lambda_i, i = 1, 2, 3, \dots, 12$, as follows, the detail of whose derivation being omitted for being straight forward.

$$\lambda_1 = -\frac{c}{\varepsilon_v}, \lambda_2 = -\frac{c}{\varepsilon_i}, \lambda_3 = -\frac{c}{\mu_v}, \lambda_4 = -\frac{c}{\mu_i}, \lambda_5 = \frac{\gamma_v}{c},$$

$$\lambda_6 = \frac{\gamma_i}{c}, \tilde{\lambda}_7 = \frac{d_v + r_v}{c}, \tilde{\lambda}_8 = \frac{d_i + r_i}{c}, \lambda_9 = \lambda_{10} = -\frac{1}{c}, \lambda_{11} = \lambda_{12} = 0.$$

Since some of the eigenvalues are positive and some are negative, the steady state $\omega 1$ is unstable, behaving like a saddle point on each phase plane.

Corresponding to $\omega 2$, for some fixed values c_5 of \tilde{y}_5 and c_6 of \tilde{y}_6 , one finds the Jacobian matrix about $\omega 2$ to have the eigenvalues $\tilde{\lambda}_i, i = 1, 2, 3, \dots, 12$, which are identical to the corresponding eigenvalues of the Jacobian matrix about $\omega 1$, except for $\tilde{\lambda}_7$ and $\tilde{\lambda}_8$, which are

$$\tilde{\lambda}_7 = \frac{d_v + r_v - \alpha_v c_5}{c}, \tilde{\lambda}_8 = \frac{d_i + r_i - \alpha_i c_6}{c} + \frac{\alpha_v \alpha_i c_5 c_6}{|c|(d_v + r_v - \alpha_v c_5)}.$$

Thus, again some of the eigenvalues are positive, while the others are negative and hence, the steady state $\omega 2$ is also unstable and behaves like a saddle point on each phase plane.

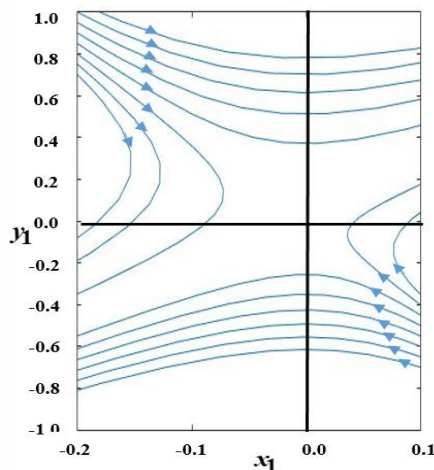


Fig. 1. Contour plots in the (x_1, y_1) phase plane. The steady state at the origin is seen to be a saddle point.

In Fig. 1. we show the contour plots in the (x_1, y_1) -plane, where $(0,0)$ is a saddle point as predicted. State variables are seen to initially approach 0 along each trajectory, but eventually get repulsed away from the saddle point $(0,0)$ as time passes.

In the next section, we derive the analytical solution to the model system (11) – (16) in the form of traveling wave fronts by utilizing the extended hyperbolic tangent method based on the work of Taghizadeh and Mirzazadeh [10].

IV. TRAVELING WAVE FRONTS

In this section, we shall employ the modified extended tanh method [16] to acquire analytical solutions in terms of the traveling wave coordinate $\xi = x - ct$. This method has been utilized in many pieces of research work [16], [17], [18] concerning important phenomena of great interest, and we refer the readers to these articles for more detailed background, development as well as its applications.

A. Analytical Solution

To this end, we attempt to find the solution of the model system (11) – (16) expressed as a finite series of hyperbolic tangent functions in the form

$$i_v = \sum_{k=0}^K a_k \phi^k, \tag{35}$$

$$i_i = \sum_{l=0}^L b_l \phi^l, \tag{36}$$

$$s_v = \sum_{m=0}^M c_m \phi^m, \tag{37}$$

$$s_i = \sum_{n=0}^N d_n \phi^n, \tag{38}$$

$$g_v = \sum_{p=0}^P e_p \phi^p, \tag{39}$$

$$g_i = \sum_{q=0}^Q f_q \phi^q, \tag{40}$$

where a_k, b_l, c_m, d_n, e_p and f_q are constants, and $\phi(\xi) = \tanh(\mu\xi)$ satisfies the Riccati equation

$$\phi' = \mu(1 - \phi^2).$$

Equating the highest orders of ϕ in (17), we are led to

$$K + 2 = K + P = L + P, \tag{41}$$

which gives $K = L, P = 2$. Equating the highest orders of in (18) leads to

$$L + 2 = K + Q = L + Q, \tag{42}$$

which gives $K = L, Q = 2$. Equating the highest orders of ϕ in (19) gives

$$M + 2 = K + P = L + P, \tag{43}$$

which gives $M = K$. Equating the highest orders of ϕ in (20) yields

$$N + 2 = L + Q = K + Q, \tag{44}$$

which gives $N = K$. Equating the highest orders of ϕ in (21) leads to

$$P+2=M, \tag{45}$$

which yields $M = 4$. Finally, equating the highest orders of ϕ in (22) leads to

$$Q+2=N, \tag{46}$$

which yields $N = 4$. Thus, we have discovered that

$$K=4, L=4, M=4, N=4, P=2 \text{ and } Q=2. \tag{47}$$

Substituting (47) into (35) – (40), we are led to the following expressions

$$i_v = a_0 + a_1\phi + a_2\phi^2 + a_3\phi^3 + a_4\phi^4, \tag{48}$$

$$i_i = b_0 + b_1\phi + b_2\phi^2 + b_3\phi^3 + b_4\phi^4, \tag{49}$$

$$s_v = c_0 + c_1\phi + c_2\phi^2 + c_3\phi^3 + c_4\phi^4, \tag{50}$$

$$s_i = d_0 + d_1\phi + d_2\phi^2 + d_3\phi^3 + d_4\phi^4, \tag{51}$$

$$g_v = e_0 + e_1\phi + e_2\phi^2, \tag{52}$$

$$g_i = f_0 + f_1\phi + f_2\phi^2. \tag{53}$$

Substituting $\phi(\xi) = \tanh(\mu\xi)$ and the Riccati equation in equations (11) – (16), with the aid of (48) – (53), and equating the coefficients of terms of equal powers of ϕ on both sides of each of the equations, we are led to the following system of algebraic equations that relate the coefficients in the series (48) – (53) together. Upon further manipulations, we are able to express all of the coefficients in terms of a_3 , b_3 and b_4 , as follows:

$$a_0 = \frac{1}{\delta_1} [c\mu a_1 + 2\varepsilon_v \mu^2 a_2 + c\mu c_1 + 2\mu_v \mu^2 c_2], \quad a_1 = -a_3,$$

$$a_2 = -\frac{160c^2 \mu^4 \mu_v}{\alpha_v \gamma_v} - \frac{4}{3} b_4,$$

$$a_4 = \frac{120c^2 \mu^4 \mu_i}{\alpha_i \gamma_i} - b_4,$$

$$b_0 = r_v a_0 + c\mu b_1 + 2\varepsilon_i \mu^2 b_2 + c\mu d_1 + 2\mu_i \mu^2 d_2,$$

$$b_1 = -\frac{2r_v}{d_i} a_3 - b_3,$$

$$b_2 = \frac{160c^2 \mu^4 r_v \mu_i}{\alpha_i \gamma_i d_i} + \frac{r_v}{d_i} a_2 + \frac{2c\mu r_v}{d_i^2} a_3 - \frac{4\delta_1}{3d_i} b_4,$$

$$c_0 = -c_2 - \frac{6c^2 \mu^2}{\gamma_v} e_2,$$

$$c_1 = \frac{40c^3 \mu^3 \delta_2}{\alpha_v \gamma_v \mu_v^2} + (\delta_2 + 1)a_3 - \frac{c\delta_2}{3\mu\mu_v} b_4,$$

$$c_2 = \frac{20c^2 \mu^2}{\alpha_v \gamma_v \mu_v^3} (\mu_v^3 \delta_1 - c^2 \delta_2) - (\delta_2 + 1)a_2 + \delta_2 \left(-\frac{c}{2\mu\mu_v} a_3 + \frac{c^2}{6\mu^2 \mu_v^2} b_4 \right) + \frac{\delta_1}{6\mu^2 \mu_v} b_4,$$

$$c_3 = -c_1,$$

$$c_4 = -120 \frac{\varepsilon_v c^2 \mu^4}{\alpha_v \gamma_v} + (\delta_2 + 1)b_4,$$

$$d_0 = -d_2 - \frac{6c^2 \mu^2}{\gamma_i} f_2,$$

$$d_1 = (\delta_4 + 1)b_3 + \frac{c\delta_4}{3\mu\mu_i} b_4,$$

$$d_2 = -\frac{20c^2 \mu^2 r_v}{\alpha_i \gamma_i} - (\delta_4 + 1)b_2 - \frac{c\delta_4}{2\mu\mu_i} b_3 + \left(\frac{\delta_3}{6\mu^2 \mu_i} - \frac{c^2 \delta_4}{6\mu^2 \mu_i^2} \right) b_4,$$

$$d_3 = -d_1, \quad d_4 = -(\delta_4 + 1)b_4,$$

$$e_1 = \left(\frac{20\varepsilon_v \mu \gamma_v}{c\alpha_v} - \frac{20c\mu\delta_2}{\alpha_v \mu_v^2} \right) - \frac{(\delta_1 + 1)\gamma_v}{2c^2 \mu^2} a_3 + \left(\frac{\delta_2 \gamma_v}{6c\mu^3 \mu_v} - \frac{(\delta_2 + 1)\gamma_v^2}{6c^3 \mu^3} \right) b_4,$$

$$e_2 = -\frac{20\varepsilon_v \mu^2}{\alpha_v} + \frac{(\delta_1 + 1)\gamma_v}{6c^2 \mu^2} b_4$$

$$f_1 = -\frac{\varepsilon_i \gamma_i}{2c^2 \mu^2} b_3 + \left(\frac{(\delta_4 + 1)\gamma_i^2}{2c^3 \mu^3} - \frac{\delta_4 c \gamma_i}{6c^2 \mu^3 \mu_i} \right) b_4,$$

$$f_2 = -\frac{(\delta_4 + 1)\gamma_i}{6c^2 \mu^2} b_4,$$

where $\delta_1 = d_v + r_v$, $\delta_2 = \frac{\varepsilon_v}{\mu_v} - 1$, $\delta_3 = d_i + r_i$, $\delta_4 = \frac{\varepsilon_i}{\mu_i} - 1$,

with e_0 and f_0 arbitrary, under the condition

$$\frac{\mu_i}{\alpha_i \gamma_i} = \frac{\mu_v}{\alpha_v \gamma_v}.$$

Thus, with the help of these equations, once we fix the values of b_0, b_2, b_4 , the values of the remaining coefficients are automatically set. Then, the coefficient values obtained in this manner can be substituted into the expressions for the state variables i_v, i_i, s_v, s_i, g_v , and g_i in (48) – (53), the plots of which provide us with the view of the wave fronts of infected and susceptible populations traveling through space and time.

B. Traveling Waves

In Fig. 2 and Fig. 3, we show the plots of the state variables modeled by equations (11) – (16) derived in terms of the traveling wave coordinate $\xi = x - ct$.

For each state variable, if we would like to see the distribution of infected individuals along different spatial locations at a certain point in time, we fix t at a constant value and vary x . For example, the graph of (48) obtained from plotting I_v against x describes a single wave front along which curve t is fixed. By plotting a series of wave fronts for different values of t , we obtain the picture of waves of infection front traveling with time, as t increases.

In Fig. 2, the plots of I_v , and I_i , are shown in 2a) and 2b), respectively, while in Fig. 3, plots of S_v and S_i are shown in Fig. 3a) and 3b), respectively, with t ranging from 0 (blue) to 80 (green), in steps of 20 units of time. For each fixed t , a front is obtained, which then travels from right to left as t increases from 0 to 80.

Fig. 4. shows 3-dimensional pictures of the state variables plotted against both temporal dimension t and spatial dimension x . With a 3-dimensional view, it can be clearly observed how the levels would rise or fall as we move along the direction in which both time and distance are changing simultaneously.

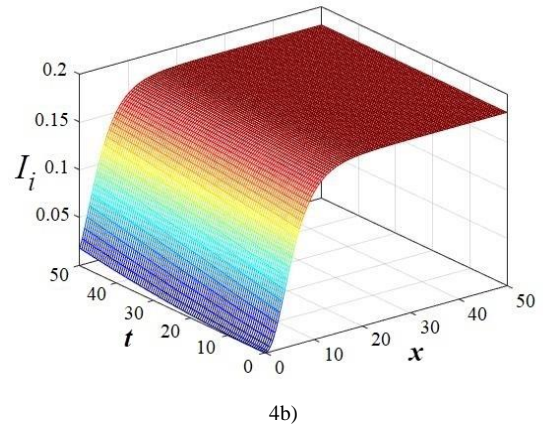
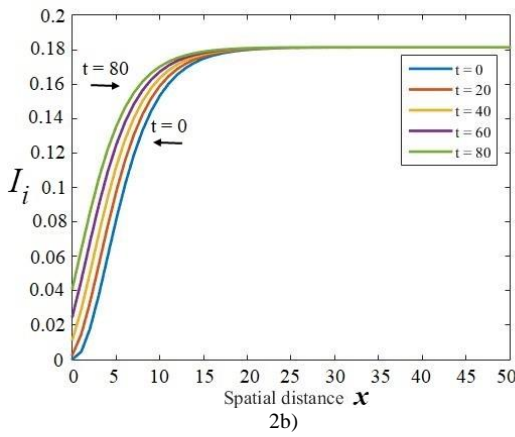
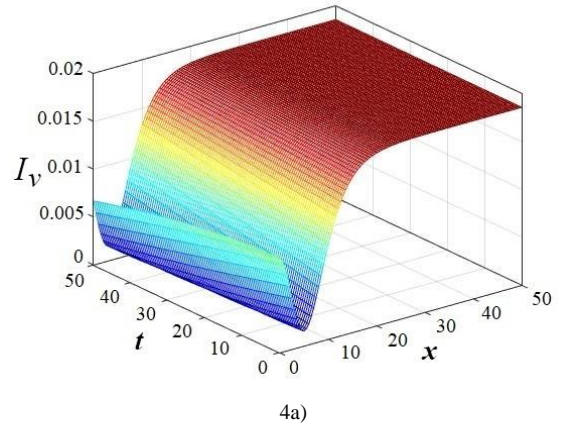
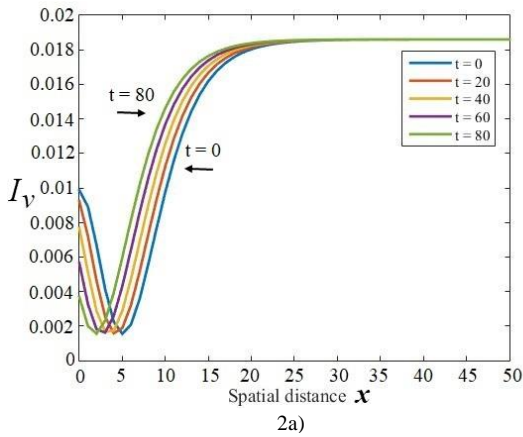


Fig. 2 Traveling wave fronts for a) I_v and b) I_i , plotted against spatial distance x for time increasing from 0 to 80, in steps of 20 units of time.

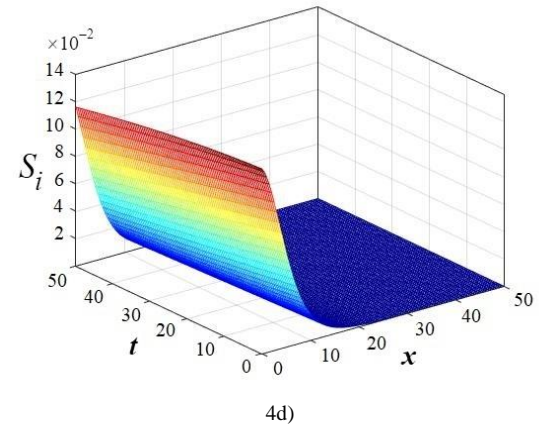
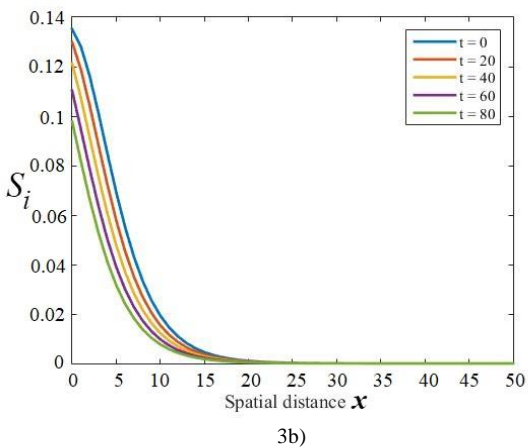
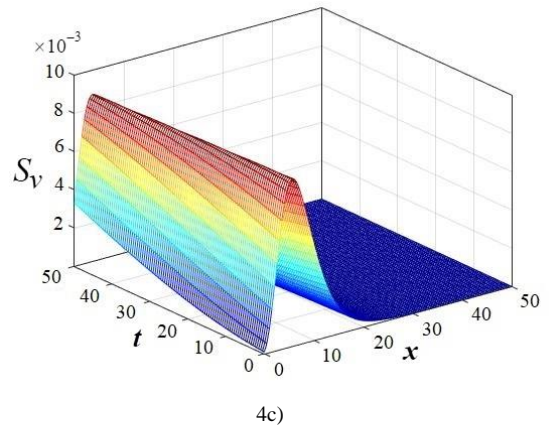
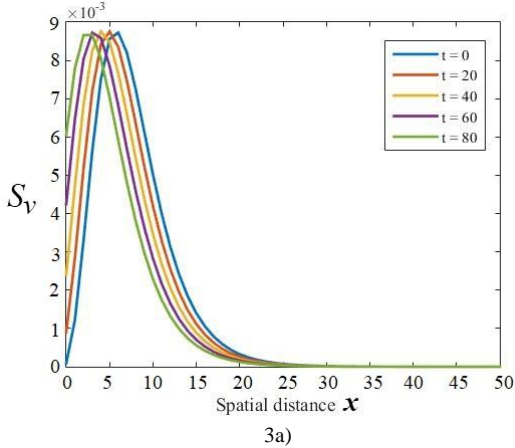


Fig. 3 Traveling wave fronts for a) S_v and b) S_i , plotted against spatial distance x for time increasing from 0 to 80, in steps of 20 units of time.

Fig. 4 Three dimensional plots of the analytic solution of the model equations (11) – (16), showing a) I_v , b) I_i , c) S_v , and d) S_i , against time t and distance x , using the same parametric values as in Fig. 2 and 3.

In Fig. 2 – 4, $\alpha_v=0.04$, $\alpha_i=0.02$, $\gamma_i=0.025$, $\gamma_v=0.05$, $\varepsilon_v=0.5$, $\varepsilon_i=0.1$, $\mu_v=0.8$, $\mu_i=0.2$, $\mu=0.15$, $c_i=-0.04$, $r_v=0.0175$, $d_v=0.0005$, $r_i=0.9999$, and $d_i=0.0004$.

The infection dynamics modeled by (1) – (6) using the above parametric values, evident in the graphs shown in Fig. 2 – 4, will be analyzed and interpreted in the next section.

V. EVALUATION AND DISCUSSION

A. Clinical Interpretation

Note that we have used the value of $\alpha_v=0.04$, which is bigger than $\alpha_i=0.02$, and $\gamma_i=0.025$ which is smaller than $\gamma_v=0.05$, so that the individuals that have been infected previously exhibit better immunity to reinfection in that it declines more slowly with time and they are infected at the smaller specific rate of infection. The values of ε_i and ε_v are set lower than those of μ_i and μ_v , respectively, since those individuals who are infectious should keep themselves relatively isolated and reduce their movement and the chance to contact and infect others, while those who have been vaccinated might feel they could be going about their business more freely than those who have not been infected previously. Those who have been infected before are expected to exhibit faster recovery from re-infection than those who have been vaccinated but not having been infected previously. Thus, $r_v=0.0175$ is much smaller than $r_i=0.9999$ in the scenario shown in Fig. 2 – 4. On the other hand, the re-infected individuals should have a much lower morbidity than those who have not been infected before, and thus $d_i=0.0004$ is smaller than $d_v=0.0005$ in this scenario.

In such a scenario the analytical solution seen in Fig. 2 – 3. is expected to reflect the infection progression that takes into account the clinical observation that persons who have been infected with SARS-CoV-2 acquire infection-induced immunity which results in reduction in severe symptoms leading to higher recovery rate and less morbidity than those not having been previously infected although vaccinated.

Closer inspection of the wave fronts in Fig. 2 and Fig. 3 allows us to make some interesting observations. Upon comparing the graphs of I_v and I_i in Fig. 2, we see that, near to the center of infection (x small), the number of infected cases I_v , derived from those vaccinated without prior infection, drops at first. This is perhaps due to the fact that, at this point in time, the number of susceptible vaccinated individuals S_v is small so that the number of this population getting infected is smaller than the number of those who have recovered. As time passes, however, the density of the susceptible vaccinated population S_v increases, as seen in Fig. 3a), so that they give rise to more infections and I_v eventually increases to a high level as a result.

On the other hand, the level of infection of individuals I_i , who have been previously infected, increases monotonically

as time progresses, since S_i starts off high in this scenario, there being many who have been infected previously. Eventually, both I_v and I_i tend asymptotically to more or less that same level.

Upon comparing the graphs of S_v and S_i in Fig. 3, we observe that, S_v starts off small since not many people have been vaccinated, but μ_v is high and this mobility causes the initial increase in S_v . However, due to weaker and waning immunity, its level eventually decreases to close to zero. On the other hand S_i decreases monotonically but at a slower rate than S_v because it takes more time to reach zero than S_v . In this particular scenario, therefore, it appears that pre-infection provides better protection against new infection than vaccination-induced immunity.

Following the above inspection of the derived analytical solutions, we are assured that our model can reflect relatively well the realistic progression of SARS-CoV-2 we might wish to use the model to simulate. Experimenting with different parametric values would be able to elucidate other scenarios of interest, which can shed more lights onto the progression dynamics of this disease.

B. Predictive Power

To further illustrate the predictive power of our model when a key parameter takes up different values to reflect various scenarios we might encounter in the future, we first investigate the effect that different values of γ_v may have on the maximum value attained by the density of susceptible vaccinated population S_v , and the effect on the minimum value reached by the density of infected population I_v , derived from those who have been vaccinated.

In Fig 5, the highest level $MaxS_v$ to which S_v rises as time progresses is plotted against the value of γ_v used in the simulation. We observe that S_v increases to a higher level, the higher γ_v gets. We recall that a higher value of γ_v indicates that immunity provided by pre-vaccination wears off faster, and hence, there are more vaccinated people susceptible to the infection in comparison to the case when γ_v is low. This highest value of the density S_v , $MaxS_v$, is seen here to increase to approximately 9.15×10^{-3} as γ_v ranges from 0.05 to 0.07.

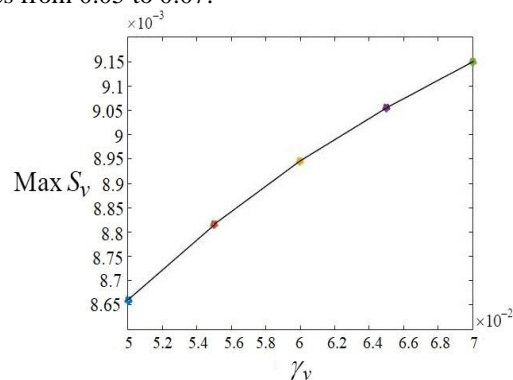


Fig. 5 The plot of $Max S_v$, the highest level reached by the density of population of individuals susceptible to infection, derived from those having been vaccinated but not previously infected, against γ_v .

In Fig. 6, we see that we can expect the lowest level $\text{Min}I_v$, to which the density of infected vaccinated population, I_v , drops, to also increase with larger γ_v , because the immunity provided by vaccination drops faster with bigger γ_v , at least up to a certain value of γ_v . After such a point, the increase in the susceptible population recovered from infection means less people in the S_v pool to be infected. This could give rise to less infection cases arising from individuals who have not been infected earlier, and hence the observed drop in $\text{Min}I_v$.

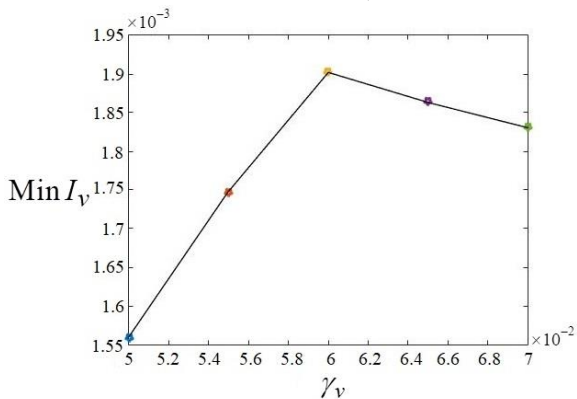


Fig. 6 The plot of $\text{Min} I_v$, the lowest level reached by the density of population of individuals infected by the virus, derived from those having been vaccinated but not previously infected, against γ_v , ranging from 0.05 to 0.07.

Next, we evaluate the model's performance through varying γ_i , which is the parameter that reflects how fast the immunity effect, provided by prior infection, wears off. Fig. 7 shows the plot, against γ_i , of the difference ΔI_i , in I_i ,

$$\Delta I_i \triangleq I_i(0, 80) - I_i(0, 0).$$

Thus, ΔI_i tells us how much I_i drops from its value at the time $t = 0$ to its value at the time $t = 80$, at the point $x = 0$ is space. We observe that as γ_i increases, ΔI_i decreases monotonically, which is as we expect, since the higher γ_i gets, the immunity wears off faster, and hence the density of infected population I_i drops more slowly. Over the same period of 80 units in time, the drop ΔI_i in I_i is smaller for larger γ_i .

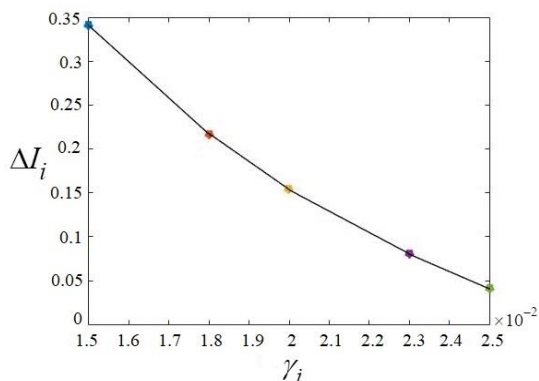


Fig. 7 The plot of ΔI_i , the drop, at $x=0$ over the period of 80 units in time, in the density of population of individuals infected by the virus, derived from those having been infected earlier, against γ_i , ranging from 0.015 to 0.025.

In Fig. 8, the difference ΔS_i in S_i , the density of previously infected susceptible population, is plotted against γ_i , ranging from 0.015 to 0.025, where

$$\Delta S_i \triangleq S_i(0, 0) - S_i(0, 80).$$

If $\Delta S_i > 0$, it tells us that after 80 units in time have passed, $S_i(0, 0) > S_i(0, 80)$, and hence the density becomes smaller at $t = 80$ than at the start $t = 0$.

Now, this difference ΔS_i is seen to be still positive but decrease as γ_i increases in Fig. 8, which means the level $S_i(0, 80)$, after 80 units in time, is still smaller than the beginning level $S_i(0, 0)$ but the gap between these levels becomes smaller due to the fact that the immunity provided by prior infection wears off faster with larger γ_i , resulting in more people becoming susceptible to infection at this position in space. Thus, our model appears to behave as it should.

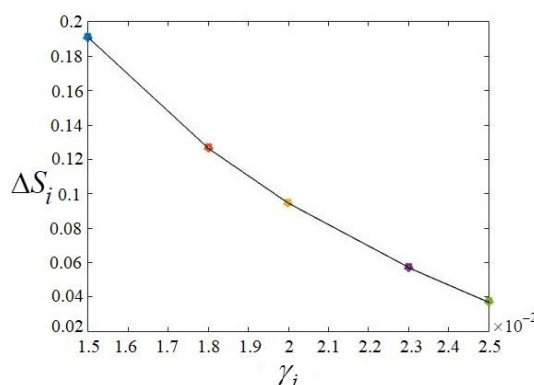


Fig. 8 The plot of ΔS_i , the difference, at $x=0$ over the period of 80 units in time, in the density of population of susceptible individuals, earlier infected by the virus, against γ_i , ranging from 0.015 to 0.025.

We can experiment, in a similar manner, with several other key parameters in our model to discover such complicated dynamics which the model is able to capture. Such complexity appears to be inherent in our model which renders it a useful and valuable tool able to provide much needed information to the decision makers in a timely fashion concerning the progression of the pandemic in the absence of vaccination or when a great deal of the population has already been infected.

VI. CONCLUSION

There is no dispute that COVID-19 pandemic has turned out to be an unprecedented global health crisis, growing in its economic, social and health impact. According to [19], mathematical models have played a crucial role in the COVID-19 crisis. Public policy decision makers have been relying on discoveries arising from mathematical modeling to inform public policies. Conclusions reached by the utilization of models have been instrumental in many of the social distancing measures that were adopted to various degrees by nations globally.

Epidemiology models of COVID-19 have seen widespread use in the efforts of decision makers to respond to a wide range of policy problems. As explained in [19], generally the type and form of models chosen in epidemiology depends on what phase the society is, in the

epidemic. Early on before it became a full-blown epidemic, models have been used for planning appropriate responses in the event of the pandemic. Decision makers would be interested to know where and how the pandemic started, what is the risk of its spread in the region, as well as basic understanding of the virus and its biomedical characteristics. As the pandemic grabbed hold, epidemiologists began to discover various strategic options of intervention and control. Moreover, greater scrutiny was paid to the forecast of the epidemic incidence rate, hospitalization rate and mortality rate, which are important information for efficient allocation of medical resources and service. Once the pandemic begins to abate, modelers now turn their attentions to developing models related to recovery and long term impacts of the instituted policies during the pandemic, such as comparative benefits or limitations related to vaccination policy, long term comorbidity symptoms, economic downfall and so on.

However, forecasting has been leaning heavily on the utilization of data driven methods. Short term forecasts have been generally reasonable, as Adiga et al. claimed in their review [19] of some of the consequential mathematical models in usage to support the continued planning and response endeavor. Although there is still intense interest in the pandemic, and a lot of data has recently become available for modelers to use in validating some of their models further, it remains very difficult to obtain real-time data on behavioral adaptation and compliance so that this is still one of the principle modeling challenges faced by modelers of the pandemic [19].

Yet, dynamic modeling, such as that described here, is valuable in the forecasting effort since the models can be used to answer, in a qualitative manner, the “what if” questions, that is, to investigate scenarios that do not currently occur or exist.

Ongoing and future investigation involves further varying of the parametric values in our model to fit with observations reported in literature concerning the dissimilar responses and immunity to coronavirus, and modification of the model to incorporate other influential factors, which will provide new and insightful information that should be valuable for many concerned parties, whether it was the policy makers or frontline responders in the field.

With rapidly evolving pandemic and unprecedented need for fast response reactions, modelers face challenges related to availability of data. Despite these challenges, however, we are certain that mathematical models can provide much needed information to the decision makers in a timely fashion concerning the progression of the pandemic as well as long term symptoms experienced by recovered patients, in order to make informed decisions on the design of public health measures and investigate various what-if scenarios.

ACKNOWLEDGMENT

The authors would like to thank Professor Andrea de Gaetano of the BioMathematics Lab, CNR IASI, Rome, Italy, and Dr. Permyos Ruengsakulrach, MD, of the Bangkok Heart Hospital, Thailand, for their valuable advice and insightful suggestions.

REFERENCES

[1] S. Nurmaini, A. E. Tondas, R. U. Partan, M. N. Rachmatullah, A. Darmawahyuni, F. Firdaus, B. Tutuko, R. Hidayat, A. I. Sapitri, “Automated detection of COVID-19 infected lesion on computed

tomography images using faster-RCNNs,” *Engineering Letters*, vol. 28, no. 4, pp. 1295-1301, 2020.

[2] M. Lamlili E.N., M. Derouch, A. Boutayeb, “A SIAR model of COVID-19 with control,” *Engineering Letters*, vol. 30, no. 1, pp. 98-107, 2022.

[3] C. Zhang, “Supporting decision-making for COVID-19 outbreaks with the modified SEIR model,” *IAENG International Journal of Computer Science*, vol. 48, no. 1, pp. 86-95, 2021.

[4] N. Yudistira, “COVID-19 growth prediction using multivariate long short term memory,” *IAENG International Journal of Computer Science*, vol. 47, no. 4, pp. 829-837, 2020.

[5] F. Yanuar, M. O. Shobri, R. F. Mabur, I.H. Putri, A. Zetra, “Classification of death risk for COVID-19 patients using Bayesian Logistic Regression and Naive Bayes Classifier,” *IAENG International Journal of Computer Science*, vol. 50, no. 3, pp. 915-920, 2023.

[6] A. A. Syed, F.L. Gaol, W. Suparta, E. Abdurachman, A. Trisetyarso, T. Matsuo, “Prediction of the impact of COVID-19 vaccine on public health using Twitter,” *IAENG International Journal of Computer Science*, vol. 49, no. 1, pp. 19-29, 2022.

[7] H. Chemaitelly, H. H. Ayoub, S. AlMukdad, P. Coyle, P. Tang, and H. M. Yassine, “Protection from previous natural infection compared with mRNA vaccination against SARS-CoV-2 infection and severe COVID-19 in Qatar: a retrospective cohort study,” *The Lancet Microbe*, vol. 3, no. 12, pp. 944-995, 2022.

[8] N. Kojima, N. K. Shrestha, and A. Klausner, “A systematic review of the protective effect of prior SARS-CoV-2 infection on repeat infection,” *Eval Health Prof.*, vol. 44, no. 4, pp. 327-332, 2021.

[9] S. Pilz, V. Theiler-Schwetz, C. Trummer, R. Krause, and J.P.A. Ioannidis, “SARS-CoV-2 reinfections: overview of efficacy and duration of natural and hybrid immunity,” *Environ Res.*, vol. 209, pp. 1-10, 2022.

[10] L. J. Abu-Raddad, H. Chemaitelly, and R. Bertollini, “Severity of SARS-CoV-2 reinfections as compared with primary infections,” *N. Engl. J. Med.*, vol. 385, pp. 2487-2489, 2021.

[11] K. A. Holder, D. P. Ings, D. O. A. Harnum, R. S. Russell, and M. D. Grant, “Moderate to severe SARS-CoV-2 infection primes vaccine-induced immunity more effectively than asymptomatic or mild infection,” *npj Vaccines*, vol. 7, no. 1, pp. 1-13, 2022.

[12] N. Pooley, S. S. A. Karim, B. Combadiere, E. E. Ooi, R. C. Harris, C. E. G. Seblain, M. Kisomi, and N. Shaikh, “Durability of vaccine-induced and natural immunity against COVID-19: a narrative review,” *Infect. Dis. Ther.*, vol. 12, no. 2, pp. 367-387, 2023.

[13] C. Hernandez-Suarez, and E. Murillo-Zamora, “Waning immunity to SARS-CoV-2 following vaccination or infection”, *Front. Med.*, vol. 9, 2022.

[14] H. Sun, editor, *Advanced Production Decline Analysis and Application*, Science Direct, 2015. Available: <https://doi.org/10.1016/C2014-0-01693-0>.

[15] J. Suksamran, Y. Lenbury, P. Satiracoo, and C. Rattanukul, “A model for Porcine Reproductive and Respiratory Syndrome with time-dependent infection rate: traveling wave solution,” *Advances in Difference Equations*, vol. 2017, no. 215, pp. 1-11, 2017.

[16] N. Taghizadeh, and M. Mirzazadeh, “The modified extended tanh method with the Riccati equation for solving nonlinear partial differential equations,” *Math. Aeterna*, vol. 2, no. 2, pp. 145-153, 2012.

[17] M. A. Abdou, “The extended tanh method and its applications for solving nonlinear nonlinear physical models,” *Appl. Math. Comput.* vol. 190, no. 1, pp. 988-996, 2007.

[18] H. A. Zedan, “New approach for tanh and extended-tanh methods with applications on Hirota-Satsuma equations,” *Comput. Appl. Math.*, vol. 28, no. 1, pp. 1-14, 2009.

[19] A. Adiga, D. Dubhashi, B. Lewis, M. Marathe, S. Venkatramanan, and A. Vullikanti, “Mathematical models for COVID-19 pandemic: a comparative analysis,” *J. Indian Inst. Sci.*, vol. 100, no. 4, pp. 793-807, 2020.